Eur. Phys. J. C 30, 123–133 (2003)
Digital Object Identifier (DOI) 10.1140/epjc/s2003-01194-4

THE EUROPEAN PHYSICAL JOURNAL C

Gluino pair production in high-energy photon collisions

S. Berge, M. Klasen[a]

II. Institut für Theoretische Physik, Universität Hamburg, Luruper Chaussee 149, 22761 Hamburg, Germany

Received: 5 March 2002 /
Published online: 8 July 2003 –

Abstract. We study the potential of high-energy photon colliders for the production of gluino pairs within the minimal supersymmetric standard model (MSSM). In this model, the process $\gamma\gamma \to \tilde{g}\tilde{g}$ is mediated by quark/squark box diagrams with enhancements for up-type quarks/squarks from their larger charges and for third generation squarks from their large mass splittings, generated by the mixing of left- and right-handed states. Far above threshold and in scenarios with very heavy squarks, resolved photons can contribute significantly at tree level. Taking into account the laser photon backscattering spectrum, electron and laser beam polarization effects, and current mass exclusion limits, we find that gluino pair production in high-energy photon collisions should be visible over large regions of the MSSM parameter space, contrary to what has been found for e^+e^- annihilation. In addition, the cross section rises rather steeply, so that a gluino mass determination with a precision of a few GeV should be feasible for a wide range of post-LEP benchmark points.

1 Introduction

Weak-scale supersymmetry (SUSY) is one of the most attractive extensions of the standard model (SM) of particle physics [1,2]. If it is realized in nature, SUSY particles will be discovered either at Run II of the Fermilab Tevatron [3–7] or within the first years of running at the CERN LHC [8,9]. Reconstruction of the SUSY Lagrangian and a precise determination of its free parameters will, however, require the clean environment of a linear e^+e^- collider, where in particular the masses, phases, and (electroweak) couplings of sfermions and gauginos will be determined with high accuracy [10]. However, the mass and coupling of the gluino will pose some difficulties, since the gluino couples only to strongly interacting particles and is thus produced only at the one-loop level or in multi-parton final states.

In a recent publication, we have investigated gluino pair production through triangular quark/squark loops in e^+e^- annihilation with center-of-mass energies up to 3 TeV, which may become available in the future at linear colliders like DESY TESLA or CERN CLIC [11,12]. Due to large cancellation effects, we found that promisingly large cross sections can only be expected for scenarios with large left-/right-handed up-type squark mass splittings or with large top-squark mixing and for gluino masses up to 500 GeV. Small gluino masses of 200 GeV might be measured with a precision of about 5 GeV in center-of-mass energy scans with luminosities of $100\,\mathrm{fb}^{-1}$/point. However, when both the left-/right-handed squark mass splitting and the squark mixing remain small, gluino pair production in e^+e^- annihilation will be hard to observe, even with luminosities of $1000\,\mathrm{fb}^{-1}$/year.

In this paper, we study the potential of high-energy photon colliders for the production of gluino pairs within the minimal supersymmetric standard model (MSSM). Similar studies have previously been carried out for the production of SM [13–15], MSSM [16], and double-charged Higgs bosons [17], sfermion pairs [18,19], and various other processes [20]. In the MSSM, the process $\gamma\gamma \to \tilde{g}\tilde{g}$ is mediated by quark/squark box diagrams with enhancements for up-type quarks/squarks from their larger charges and for third generation squarks from their large mass splittings, generated by the mixing of left- and right-handed states. At tree level, gluinos can be produced in pairs only in association with two quarks, or they are produced singly in association with a quark and a squark. Both processes result in multi-jet final states, where phase space is limited and gluinos may be hard to isolate. Far above threshold and in scenarios with very heavy squarks, resolved photons can contribute significantly at tree level. Taking into account the usual laser photon backscattering spectrum [21], electron and laser beam polarization effects, and current mass exclusion limits, we find that gluino pair production in high-energy photon collisions should be visible over large regions of the MSSM parameter space, contrary to what has been found for e^+e^- annihilation. In addition, the cross section rises rather steeply, so that a gluino mass determination with a precision of a few GeV should be feasible for a wide range of post-LEP benchmark points.

Our calculations involve various masses and couplings of SM particles, for which we use the most up-to-date values from the 2002 Review of the Particle Data Group [22]. In particular, we evaluate the electromagnetic fine

[a] e-mail: michael.klasen@desy.de

structure constant $\alpha(m_Z) = 1/127.934$ at the mass of the Z^0-boson, $m_Z = 91.1876\,\text{GeV}$, and calculate the weak mixing angle θ_W from the tree-level expression $\sin^2\theta_W = 1 - m_W^2/m_Z^2$ with $m_W = 80.423\,\text{GeV}$. Among the quark masses, only the one of the top quark, $m_t = 174.3\,\text{GeV}$, plays a significant role, while the bottom quark mass, $m_b = 4.7\,\text{GeV}$, and the charm quark mass, $m_c = 1.5\,\text{GeV}$, could have been neglected like those of the three light quarks. The strong coupling constant is evaluated at the gluino mass scale from the one-loop expression with five active flavors and $\Lambda_{\text{LO}}^{n_f=5} = 83.76\,\text{MeV}$, corresponding to the world avarage (available only at two loops) of $\alpha_s(m_Z) = 0.1172$. A variation of the renormalization scale by a factor of four about the gluino mass results in a cross section uncertainty of about $\pm 25\%$, which can be reduced considerably by including full next-to-leading order QCD corrections. Like the heavy top quark, all SUSY particles have been decoupled from the running of the strong coupling constant.

We work in the framework of the MSSM with conserved R- (matter-) parity, which represents the simplest phenomenologically viable model, but which is still sufficiently general to not depend on a specific SUSY breaking mechanism. Models with broken R-parity are severely restricted by the non-observation of proton decay, which would violate both baryon and lepton number conservation. We do not consider light gluino mass windows, which may or may not be excluded from searches at fixed target and collider experiments [22]. Instead, we adopt the current mass limit $m_{\tilde{g}} \geq 200\,\text{GeV}$ from the CDF [23] and D0 [24] searches in the jets with missing energy channel, relevant for non-mixing squark masses of $m_{\tilde{q}} \geq 325\,\text{GeV}$ and $\tan\beta = 3$. Values for the ratio of the Higgs vacuum expectation values, $\tan\beta$, below 2.4 are already excluded by the CERN LEP experiments, although this value is obtained using one-loop corrections only and depends in addition on the top quark mass. Furthermore, values of $\tan\beta$ between 2.4 and 8.5 are only allowed in a very narrow window of light Higgs boson masses between 113 and 127 GeV [25]. Therefore, we employ a safely high value of $\tan\beta = 10$. If not stated otherwise, we adopt the smallest allowed universal squark mass of $m_{\tilde{q}} \simeq m_{\text{SUSY}} = 325\,\text{GeV}$ and large top-squark mixing with $\theta_{\tilde{t}} = 45.195°$, $m_{\tilde{t}_1} = 110.519\,\text{GeV}$, and $m_{\tilde{t}_2} = 505.689\,\text{GeV}$, which can be generated by choosing appropriate values for the Higgs mass parameter, $\mu = -500\,\text{GeV}$, and the trilinear top-squark coupling, $A_t = 648.512\,\text{GeV}$ [26]. The SUSY one-loop contributions to the ρ-parameter and the light top-squark mass $m_{\tilde{t}_1}$ are then still significantly below and above the CERN LEP limits, $\rho_{\text{SUSY}} < 0.0012^{+0.0023}_{-0.0014}$ and $m_{\tilde{t}_1} \geq 100\,\text{GeV}$ [22,27]. For small and intermediate values of $\tan\beta$, mixing in the bottom squark sector remains small, and we take $\theta_{\tilde{b}} = 0°$ as for the four light squark flavors.

The remainder of this paper is organized as follows: In Sect. 2 we compute the one-loop amplitudes for gluino pair production in direct photon–photon collisions, discuss briefly their analytical properties, and study in detail their numerical dependence on the squark masses and mixing angles, on the photon polarization and center-of-mass energy. In Sect. 3 we calculate the squared matrix elements for the resolved photon contributions from quark–antiquark and gluon–gluon scattering analytically and discuss several typical cases, where resolved processes can be numerically important. In Sect. 4 we present expected total cross sections for gluino pair production with laser backscattered photons in polarized electron–electron collisions for various post-LEP benchmark SUSY scenarios. We then estimate the precision with which the gluino mass might be determined for various typical squark and gluino masses and realistic photon collider luminosities. Finally, our conclusions are given in Sect. 5.

2 Direct photon–photon scattering

As the supersymmetric partners of the gauge bosons of the strong interaction, gluinos couple only to colored particles and sparticles and can therefore not be pair-produced directly at tree level in photon–photon collisions. Instead, they are produed at the one-loop level through the box diagrams shown in Fig. 1, where the virtual quark/squark flavor can flow in both directions. Topologically, additional triangular loop diagrams without a quartic vertex and two-point functions with a quartic vertex are also allowed, but they evaluate to zero, since they involve internal gluon propagators and only one (traceless) color matrix inside the quark/squark loop. A full set of diagrams can be generated with the computer algebra package FeynArts [28, 29].

Denoting the four-momenta of the incoming photons with p_i^μ, their polarization vectors with $\varepsilon^\mu(p_i)$, the four-momenta of the produced gluinos with k_i^μ, and employing the Feynman rules of SUSY-QCD [2], we can write down the scattering amplitudes for the diagrams with one internal squark propagator,

$$\begin{aligned}
\mathcal{M}_{t1} = & \int \frac{\mathrm{d}^4 q}{(2\pi)^4} \mathrm{i}\varepsilon^\mu(p_1)\varepsilon^\nu(p_2) \\
& \times \Big[\overline{u}(k_1, m_{\tilde{g}}) \left(-\mathrm{i}\sqrt{2} g_s \omega_- T^a_{mn} S^{\tilde{q}}_{i1} + \mathrm{i}\sqrt{2} g_s \omega_+ T^a_{mn} S^{\tilde{q}}_{i2}\right) \\
& \times (-\not{p}_2 - \not{q} + \not{k}_1 + \not{k}_2 + m_q) (-\mathrm{i}e e_q \gamma^\mu) (-\not{q} + m_q) \\
& \times (-\mathrm{i}e e_q \gamma^\nu) (-\not{p}_2 - \not{q} + m_q) \\
& \times \left(\mathrm{i}\sqrt{2} g_s S^{\tilde{q}\,\dagger}_{i2} \omega_- T^b_{nm} - \mathrm{i}\sqrt{2} g_s S^{\tilde{q}\,\dagger}_{i1} \omega_+ T^b_{nm}\right) v(k_2, m_{\tilde{g}})\Big] \\
& / \Big[\left(q^2 - {m_q}^2\right) \left((p_2 + q)^2 - {m_q}^2\right) \\
& \times \left((p_2 + q - k_2)^2 - {m_{\tilde{q}_i}}^2\right) \\
& \times \left((p_2 + q - k_1 - k_2)^2 - {m_q}^2\right)\Big], \qquad (1)
\end{aligned}$$

$$\begin{aligned}
\mathcal{M}_{u1} = & \int \frac{\mathrm{d}^4 q}{(2\pi)^4} \mathrm{i}\varepsilon^\mu(p_1)\varepsilon^\nu(p_2) \\
& \times \Big[\overline{u}(k_1, m_{\tilde{g}}) \left(\mathrm{i}\sqrt{2} g_s S^{\tilde{q}\,\dagger}_{i2} \omega_- T^a_{mn} - \mathrm{i}\sqrt{2} g_s S^{\tilde{q}\,\dagger}_{i1} \omega_+ T^a_{mn}\right) \\
& \times (\not{p}_2 + \not{q} + m_q) \\
& \times (\mathrm{i}e e_q \gamma^\nu) (\not{q} + m_q) (\mathrm{i}e e_q \gamma^\mu) (\not{p}_2 + \not{q} - \not{k}_1 - \not{k}_2 + m_q)
\end{aligned}$$

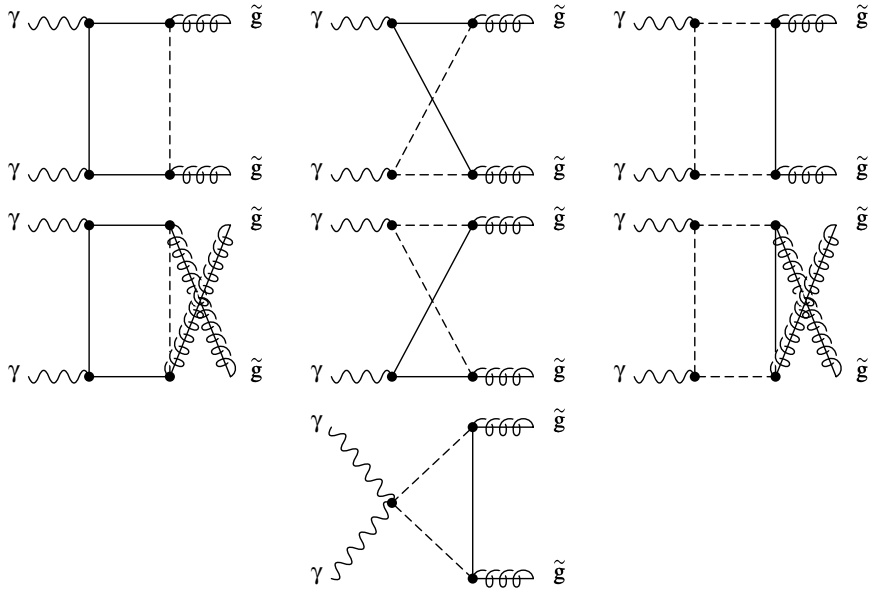

Fig. 1. Feynman diagrams for gluino pair production in direct photon–photon collisions. The photons couple to the produced gluinos through quark (full lines) and squark (dashed lines) box diagrams with flavor flow in both directions

$$\times \left(-\mathrm{i}\sqrt{2}g_s\omega_- T^b_{nm} S^{\tilde{q}}_{i1} + \mathrm{i}\sqrt{2}g_s\omega_+ T^b_{nm} S^{\tilde{q}}_{i2}\right) v(k_2, m_{\tilde{g}})\Big]$$
$$/\ \Big[\left(q^2 - {m_q}^2\right)\left((p_2+q)^2 - {m_q}^2\right)$$
$$\times \left((p_2+q-k_1)^2 - {m_{\tilde{q}_i}}^2\right)$$
$$\times \left((p_2+q-k_1-k_2)^2 - {m_q}^2\right)\Big], \qquad (2)$$

for the diagrams with two internal squark propagators,

$$\mathcal{M}_{t2} = \int \frac{\mathrm{d}^4 q}{(2\pi)^4} e e_q (-p_2 - 2q + 2k_1)^\nu \varepsilon^\mu(p_1)\varepsilon^\nu(p_2)$$
$$\times \Big[\overline{u}(k_1, m_{\tilde{g}})\left(\mathrm{i}\sqrt{2}g_s {S^{\tilde{q}}_{i2}}^\dagger \omega_- T^a_{mn} - \mathrm{i}\sqrt{2}g_s {S^{\tilde{q}}_{i1}}^\dagger \omega_+ T^a_{mn}\right)$$
$$\times (\not{q} + m_q)\left(\mathrm{i}e e_q \gamma^\mu\right)(\not{p}_2 + \not{q} - \not{k}_1 - \not{k}_2 + m_q)$$
$$\times \left(-\mathrm{i}\sqrt{2}g_s\omega_- T^b_{nm} S^{\tilde{q}}_{i1} + \mathrm{i}\sqrt{2}g_s\omega_+ T^b_{nm} S^{\tilde{q}}_{i2}\right) v(k_2, m_{\tilde{g}})\Big]$$
$$\times /\Big[\left(q^2 - {m_q}^2\right)\left((q-k_1)^2 - {m_{\tilde{q}_i}}^2\right)$$
$$\times \left((p_2+q-k_1)^2 - {m_{\tilde{q}_i}}^2\right)$$
$$\times \left((p_2+q-k_1-k_2)^2 - {m_q}^2\right)\Big], \qquad (3)$$

$$\mathcal{M}_{u2} = \int \frac{\mathrm{d}^4 q}{(2\pi)^4}(-e e_q)$$
$$\times (p_2 + 2q - k_1 - k_2)^\mu \varepsilon^\mu(p_1)\varepsilon^\nu(p_2)$$
$$\times \Big[\overline{u}(k_1, m_{\tilde{g}})\left(-\mathrm{i}\sqrt{2}g_s\omega_- T^a_{mn} S^{\tilde{q}}_{i1} + \mathrm{i}\sqrt{2}g_s\omega_+ T^a_{mn} S^{\tilde{q}}_{i2}\right)$$
$$\times (-\not{q} + \not{k}_1 + m_q)\left(-\mathrm{i}e e_q \gamma^\nu\right)(-\not{p}_2 - \not{q} + \not{k}_1 + m_q)$$
$$\times \left(\mathrm{i}\sqrt{2}g_s {S^{\tilde{q}}_{i2}}^\dagger \omega_- T^b_{nm} - \mathrm{i}\sqrt{2}g_s {S^{\tilde{q}}_{i1}}^\dagger \omega_+ T^b_{nm}\right) v(k_2, m_{\tilde{g}})\Big]$$
$$/\ \Big[\left(q^2 - {m_{\tilde{q}_i}}^2\right)\left((q-k_1)^2 - {m_q}^2\right)$$
$$\times \left((p_2+q-k_1)^2 - {m_q}^2\right)$$
$$\times \left((p_2+q-k_1-k_2)^2 - {m_{\tilde{q}_i}}^2\right)\Big], \qquad (4)$$

$$\mathcal{M}_{x2} = \int \frac{\mathrm{d}^4 q}{(2\pi)^4} 2\mathrm{i}e^2 e_q^2 g^{\mu\nu}\varepsilon^\mu(p_1)\varepsilon^\nu(p_2)$$
$$\times \Big[\overline{u}(k_1, m_{\tilde{g}})\left(-\mathrm{i}\sqrt{2}g_s\omega_- T^a_{mn} S^{\tilde{q}}_{i1} + \mathrm{i}\sqrt{2}g_s\omega_+ T^a_{mn} S^{\tilde{q}}_{i2}\right)$$
$$\times (-\not{q} + m_q)\left(\mathrm{i}\sqrt{2}g_s {S^{\tilde{q}}_{i2}}^\dagger \omega_- T^b_{nm} - \mathrm{i}\sqrt{2}g_s {S^{\tilde{q}}_{i1}}^\dagger \omega_+ T^b_{nm}\right)$$
$$\times v(k_2, m_{\tilde{g}})\Big]/\Big[\left(q^2 - {m_q}^2\right)$$
$$\times \left((q+k_1)^2 - {m_{\tilde{q}_i}}^2\right)\left((q-k_2)^2 - {m_{\tilde{q}_i}}^2\right)\Big], \qquad (5)$$

and for the diagrams with three internal squark propagators,

$$\mathcal{M}_{t3} = \int \frac{\mathrm{d}^4 q}{(2\pi)^4}(-\mathrm{i}e^2 e_q^2)(-p_2 - 2q)^\nu$$
$$\times (-p_2 - 2q + k_1 + k_2)^\mu \varepsilon^\mu(p_1)\varepsilon^\nu(p_2)$$
$$\times \Big[\overline{u}(k_1, m_{\tilde{g}})\left(\mathrm{i}\sqrt{2}g_s {S^{\tilde{q}}_{i2}}^\dagger \omega_- T^a_{mn} + -\mathrm{i}\sqrt{2}g_s {S^{\tilde{q}}_{i1}}^\dagger \omega_+ T^a_{mn}\right)$$
$$\times (\not{p}_2 + \not{q} - \not{k}_2 + m_q)$$
$$\times \left(-\mathrm{i}\sqrt{2}g_s\omega_- T^b_{nm} S^{\tilde{q}}_{i1} + \mathrm{i}\sqrt{2}g_s\omega_+ T^b_{nm} S^{\tilde{q}}_{i2}\right) v(k_2, m_{\tilde{g}})\Big]$$
$$/\ \Big[\left(q^2 - {m_{\tilde{q}_i}}^2\right)\left((p_2+q)^2 - {m_{\tilde{q}_i}}^2\right)$$
$$\times \left((p_2+q-k_2)^2 - {m_q}^2\right)$$
$$\times \left((p_2+q-k_1-k_2)^2 - {m_{\tilde{q}_i}}^2\right)\Big], \qquad (6)$$

and

$$\mathcal{M}_{u3} = \int \frac{\mathrm{d}^4 q}{(2\pi)^4}(-\mathrm{i}e^2 e_q^2)(-p_2 - 2q)^\nu$$
$$\times (-p_2 - 2q + k_1 + k_2)^\mu \varepsilon^\mu(p_1)\varepsilon^\nu(p_2)$$
$$\times \Big[\overline{u}(k_1, m_{\tilde{g}})\left(-\mathrm{i}\sqrt{2}g_s\omega_- T^a_{mn} S^{\tilde{q}}_{i1} + \mathrm{i}\sqrt{2}g_s\omega_+ T^a_{mn} S^{\tilde{q}}_{i2}\right)$$
$$\times (-\not{p}_2 - \not{q} + \not{k}_1 + m_q)$$
$$\times \left(\mathrm{i}\sqrt{2}g_s {S^{\tilde{q}}_{i2}}^\dagger \omega_- T^b_{nm} + -\mathrm{i}\sqrt{2}g_s {S^{\tilde{q}}_{i1}}^\dagger \omega_+ T^b_{nm}\right) v(k_2, m_{\tilde{g}})\Big]$$

$$/ \left[\left(q^2 - {m_{\tilde{q}_i}}^2\right) \left((p_2+q)^2 - {m_{\tilde{q}_i}}^2\right) \right.$$
$$\times \left((p_2+q-k_1)^2 - {m_q}^2\right)$$
$$\left. \times \left((p_2+q-k_1-k_2)^2 - {m_{\tilde{q}_i}}^2\right) \right]. \quad (7)$$

Here, e and g_s are the electromagnetic and strong couplings, respectively, e_q is the fractional charge of the quark flavor q in the loop, and T^a_{mn} is the SU(3) color matrix attached to gluinos of color a, and summation over the (s)quark color indices m, n is implied. $m_{\tilde{g}}$, m_q, and $m_{\tilde{q}_i}$ are the masses of the gluino, quark, and squark mass eigenstate i, and q^μ is the internal loop momentum. For diagrams with opposite flavor flow, the projectors $\omega_\pm = (1 \pm \gamma_5)/2$ must be interchanged and the Hermitean conjugate of the squark mixing matrices $S^{\tilde{q}}_{ij}$ must be taken, so that for real (CP-conserving) squark mixing matrices the scattering amplitudes become independent of γ_5 when summed over both directions of the flavor flow. The loop integrals in (1)–(7) are free of ultraviolet divergences, since they involve at least three propagators and no tree-level coupling of the photon to the gluino that would require renormalization. They are also free of infrared and collinear singularities, since massless gluons do not appear, and are therefore most easily evaluated numerically [30–32].

After summing these amplitudes over internal quark flavors q, squark mass eigenstates i, colors and helicities of the produced gluinos, we obtain the direct photon–photon cross section

$$\sigma^{\rm dir}_{\gamma\gamma} = \frac{1}{2s_{\gamma\gamma}} \frac{1}{8\pi s_{\gamma\gamma}} \frac{1}{2} \int {\rm d}t_{\tilde{g}} \sum_{a,b} |\mathcal{M}_{\gamma\gamma}|^2, \quad (8)$$

where

$$\mathcal{M}_{\gamma\gamma} = \sum_{q=1}^{6} \sum_{i=1}^{2} (\mathcal{M}_{t1} + \mathcal{M}_{u1} + \mathcal{M}_{t2} + \mathcal{M}_{u2} + \mathcal{M}_{x2} + \mathcal{M}_{t3} + \mathcal{M}_{u3}) + (\omega_+ \leftrightarrow \omega_-\,,\, S^{\tilde{q}}_{ij} \leftrightarrow {S^{\tilde{q}}_{ij}}^\dagger), \quad (9)$$

$s_{\gamma\gamma} = (p_1+p_2)^2$, $t_{\tilde{g}} = (p_1-k_1)^2 - m^2_{\tilde{g}}$, and $u_{\tilde{g}} = (p_1 - k_2) - m^2_{\tilde{g}}$ are the mass-subtracted Lorentz-invariant Mandelstam variables, $t_{\tilde{g}}$ is integrated in the range $[-s_{\gamma\gamma} \pm \sqrt{s_{\gamma\gamma}(s_{\gamma\gamma} - 4m^2_{\tilde{g}})}]/2$, and where we have included a factor of 1/2 for the production of two identical Majorana fermions. For unpolarized cross sections, we sum in addition over the transverse polarizations T of the initial photons with the completeness relation

$$\sum_T \varepsilon^{\mu *}(p_i) \varepsilon^\nu(p_i) = -g^{\mu\nu} \quad (10)$$

and include a spin averaging factor of 1/2 for each photon. We find perfect agreement (up to ten digits) between our direct analytical and our computer algebra assisted [32] calculations.

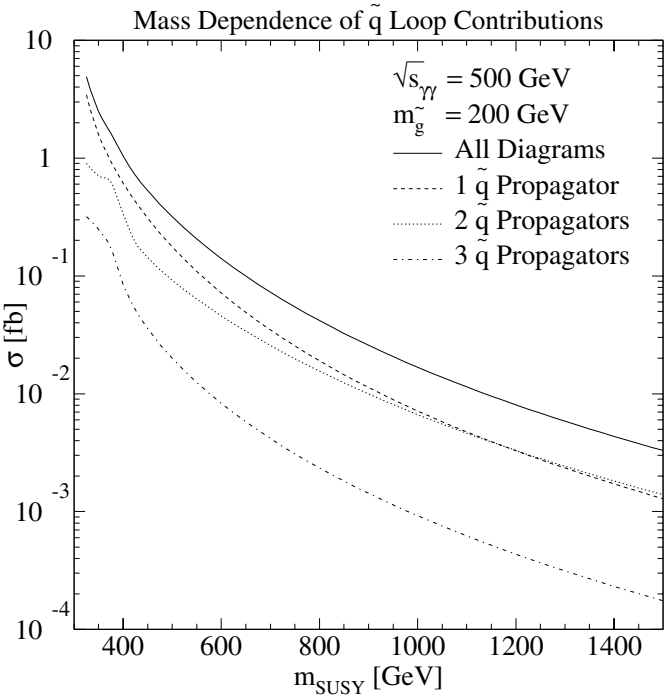

Fig. 2. Dependence of the gluino pair production cross section in unpolarized photon–photon collisions on the squark mass parameter $m_{\rm SUSY}$. The numerical importance of the amplitudes decreases with the number of internal squark propagators

As is evident from Fig. 2, the numerical importance of the amplitudes in (1)–(7) depends directly on the number of internal squark propagators, which induce a suppression with the heavy squark mass $m_{\tilde{q}}$ or, equivalently, the parameter $m_{\rm SUSY}$. The dominant contribution comes from diagrams with one internal squark propagator, but diagrams with two internal squark propagators still contribute significantly and cannot be neglected as proposed in [33]. They are even more important once the photon–photon center-of-mass energy allows for the production of two intermediate on-shell squarks, i.e. when $\sqrt{s}_{\gamma\gamma} > 2m_{\tilde{q}}$, so that real and imaginary parts of the loop diagrams contribute. Only the diagrams with three internal squark propagators are indeed of negligible impact.

The number and (s- or t-channel) nature of the squark propagators occurring in the Feynman diagrams of Fig. 1 is clearly reflected in a distinct threshold behavior, shown in Fig. 3. For example, the diagrams in the center column of Fig. 1 involve two s-channel squark propagators, which can become on-shell when $\sqrt{s}_{\gamma\gamma} \geq 2m_{\tilde{q}} \simeq 2m_{\rm SUSY}$. The same observation holds for the diagrams in the right column of Fig. 1, which are, however, suppressed by an additional t-channel squark propagator. For lighter gluinos with mass $m_{\tilde{g}} < m_t$ or $m_{\tilde{g}} < m_{\tilde{t}_1}$, similar resonance structures would be visible where the center-of-mass energy crosses the pair production threshold for top quarks and squarks. For very light gluinos of mass $m_{\tilde{g}} = 5...25\,{\rm GeV}$,

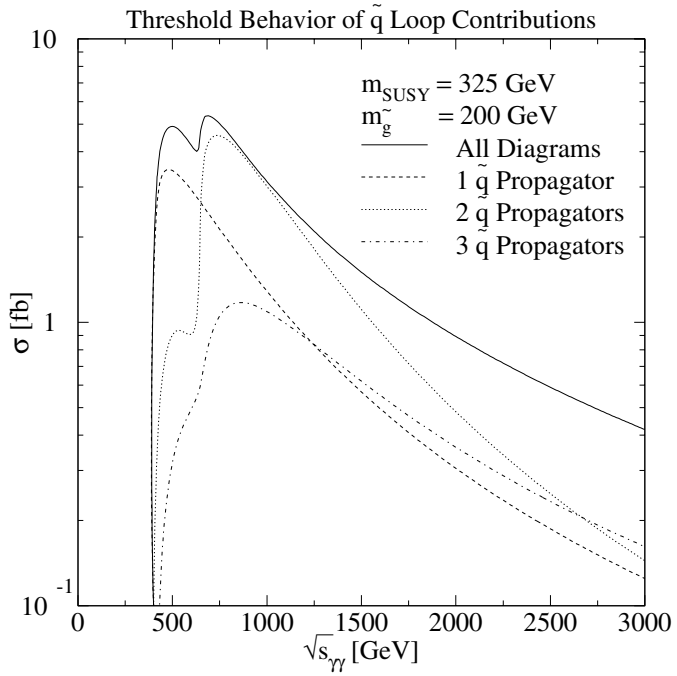

Fig. 3. Threshold behavior of the gluino pair production cross section in unpolarized photon–photon collisions for diagrams involving different numbers of squark propagators

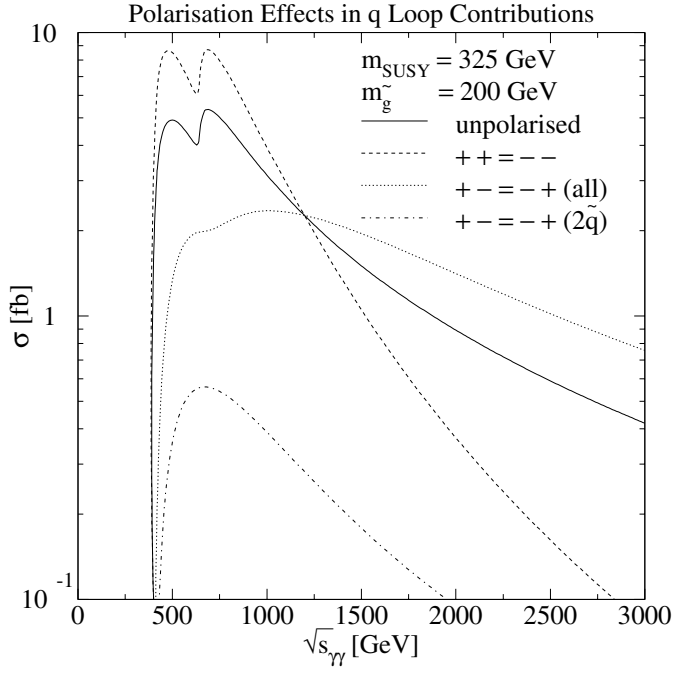

Fig. 4. Threshold behavior of the gluino pair production cross section in polarized photon–photon collisions

squarks of mass 50...150 GeV, and neglecting the diagrams with more than one squark propagator, all quark masses, and squark mixing effects, we can roughly reproduce the shapes and magnitudes (in pb, not nb) of the threshold behavior in Fig. 2 of [33]. For a more detailed numerical comparison, more information on the quark charges and coupling constants used there would be needed.

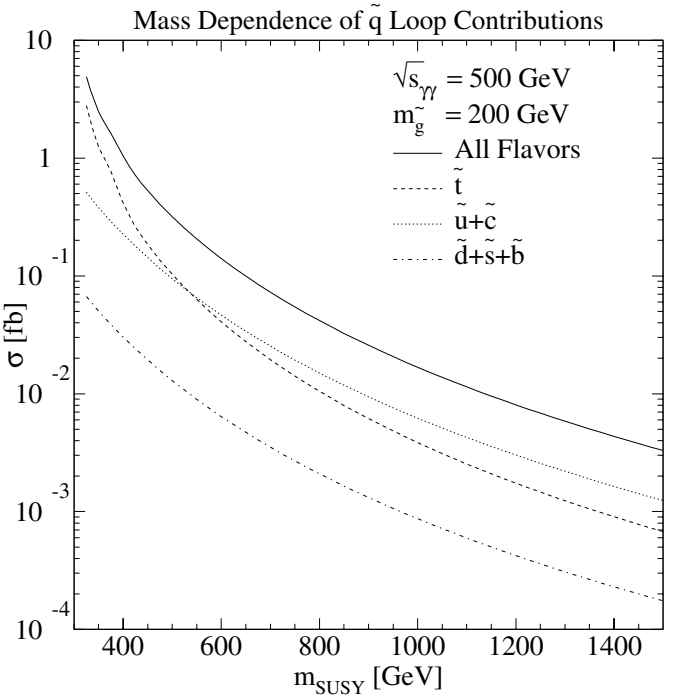

Fig. 5. Dependence of the gluino pair production cross section in unpolarized photon–photon collisions on the squark mass parameter m_{SUSY}. Down-type (d, s, and b) quarks and squarks are suppressed relative to up-type (u, c, and t) quarks and squarks due to their smaller electromagnetic charges

As can be seen in Fig. 4, the threshold behavior of the gluino pair production cross section is also influenced by the polarization of the initial photons. If they carry the same helicity, the cross section shows the steep rise typical for S-wave production of the two gluinos, whereas for photons with opposite helicity the gluinos are produced as a P-wave, the cross section rises more slowly, and the intermediate squarks in diagrams with two s-channel propagators cannot be produced on-shell (see the dot-dashed curve in Fig. 4). For center-of-mass energy scans it is therefore advantageous to choose the same helicities for both photons.

Since the cross section in (8) is proportional to the fourth power of the fractional quark charge, up-type (s)quarks contribute 16 times as much as down-type (s)quarks (see Fig. 5). In addition, the top-squark contribution is enhanced for small m_{SUSY} due to the large top-squark mixing angle and the small mass of the light top-squark mass eigenstate.

The influence of the top-squark mixing angle is shown in Fig. 6, where the central region is excluded by the CERN LEP limits on the ρ-parameter and $m_{\tilde{t}_1}$ [22,27]. It is quite strong above the excluded region, $\theta_{\tilde{t}} \geq 45.192°$, where the mass of the light top-squark mass eigenstate rises quickly from $m_{\tilde{t}_1} \geq 100\,\mathrm{GeV}$ to values around $m_{\mathrm{SUSY}} = 325\,\mathrm{GeV}$. In this region, the top-squark contribution (dashed curve) to the gluino pair production cross section drops by more than one order of magnitude, whereas the total cross section (full curve) drops only by about a factor

of four due to the interference with the constant contributions from the other, non-mixing (s)quarks (dotted curve).

3 Resolved photon–photon scattering

As the gauge boson of the electromagnetic interaction, the photon can only interact directly with charged (s)particles, so that gluino pair production arises only at one-loop and $\mathcal{O}(\alpha^2\alpha_s^2)$. However, in high-energy scattering processes the photon can also fluctuate into intermediate quark–antiquark states and develop a complex hadronic structure. The quarks and gluons inside the photon carry then only a fraction of the photon's energy. When both photons are resolved into quarks or gluons, the latter can interact strongly and gluino pairs can be produced already at tree level. These $\mathcal{O}(\alpha_s^2)$ double-resolved processes can be numerically large, despite the fact that a suppression from the $\mathcal{O}(\alpha/\alpha_s)$ quark and $\mathcal{O}(\alpha)$ gluon densities in the photon must be taken into account. If only one photon is resolved, gluino pairs are produced through the one-loop diagrams in Fig. 1 with one photon being replaced by a gluon (and the additional color-octet diagrams not shown in Fig. 1), so that they are then of $\mathcal{O}(\alpha\alpha_s^3)$. Due to their additional suppression from the $\mathcal{O}(\alpha)$ gluon density, these contributions are numerically small and will be neglected in the following.

Gluino pair production in double-resolved photon–photon scattering arises from the quark–antiquark and gluon–gluon scattering diagrams shown in Figs. 7 and 8. The corresponding spin- and color-averaged squared matrix elements are [34]

$$\overline{|\mathcal{M}_{q\bar{q}}|}^2 = \frac{2g_s^4(N_C^2-1)\ N_C}{4N_C^2} \times \left(2\frac{2m_{\tilde{g}}^2 s + t_{\tilde{g}}^2 + u_{\tilde{g}}^2}{s^2} + 2\frac{m_{\tilde{g}}^2 s + t_{\tilde{g}}^2}{s t_{\tilde{q}}} + 2\frac{m_{\tilde{g}}^2 s + u_{\tilde{g}}^2}{s u_{\tilde{q}}} + \frac{t_{\tilde{g}}^2}{t_{\tilde{q}}^2} + \frac{u_{\tilde{g}}^2}{u_{\tilde{q}}^2}\right) + \frac{2g_s^4(N_C^2-1)/N_C}{4N_C^2}\left(2\frac{m_{\tilde{g}}^2 s}{t_{\tilde{q}} u_{\tilde{q}}} - \frac{t_{\tilde{g}}^2}{t_{\tilde{q}}^2} - \frac{u_{\tilde{g}}^2}{u_{\tilde{q}}^2}\right) \tag{11}$$

and

$$\overline{|\mathcal{M}_{gg}|}^2 = \frac{8g_s^4(N_C^2-1)\ N_C^2}{4(N_C^2-1)^2}\left(1 - \frac{t_{\tilde{g}} u_{\tilde{g}}}{s^2}\right) \times \left[\frac{s^2}{t_{\tilde{g}} u_{\tilde{g}}} - 2 + 4\frac{m_{\tilde{g}}^2 s}{t_{\tilde{g}} u_{\tilde{g}}}\left(1 - \frac{m_{\tilde{g}}^2 s}{t_{\tilde{g}} u_{\tilde{g}}}\right)\right], \tag{12}$$

where $t_{\tilde{q}} = (p_1 - k_1)^2 - m_{\tilde{q}}^2$, and $u_{\tilde{q}} = (p_1 - k_2)^2 - m_{\tilde{q}}^2$ are again mass-subtracted Lorentz-invariant Mandelstam variables, p_i^μ are now the four-momenta of the incoming partons, and $N_C = 3$ denotes the number of colors. The unpolarized double-resolved photon cross section is then given by

$$\sigma_{\gamma\gamma}^{\rm res} = \sum_{i,j=q,\bar{q},g} \int \mathrm{d}x_1 f_{i/\gamma}(x_1, M^2)\mathrm{d}x_2 f_{j/\gamma}(x_2, M^2) \times \frac{1}{2s}\frac{\mathrm{d}t_{\tilde{g}}}{8\pi s}\frac{1}{2}\overline{|\mathcal{M}_{ij}|}^2, \tag{13}$$

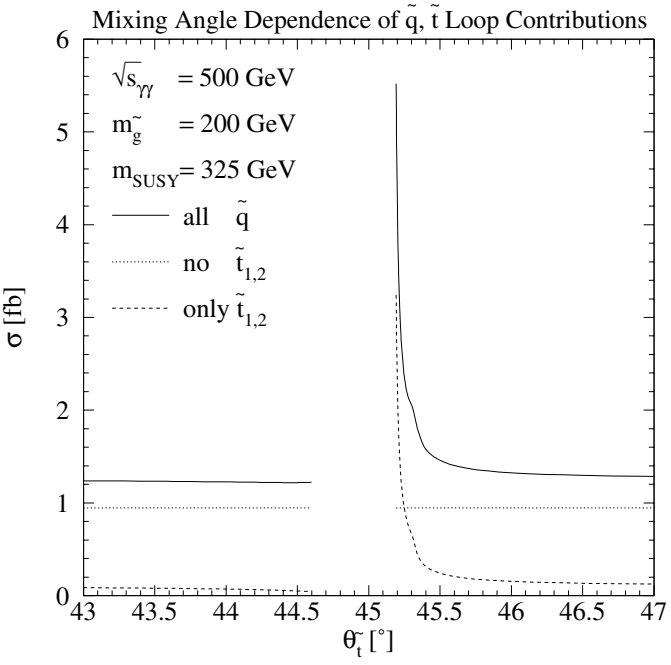

Fig. 6. Dependence of the gluino pair production cross section in unpolarized photon–photon collisions on the top-squark mixing angle

where $s = x_1 x_s s_{\gamma\gamma}$ is the partonic center-of-mass energy, $x_{1,2}$ are the longitudinal momentum fractions of the partons i and j in the photons, and M is the factorization scale, which we identify with the gluino mass. The variation of the double-resolved photon cross section with this scale, which amounts to $\pm 35\%$ in leading order for a variation of M about $m_{\tilde{g}}$ by a factor of four, will be considerably reduced, once the corresponding higher-order direct processes are included.

In contrast to the gluon–gluon initiated matrix element in (12), which involves only gluons and gluinos and depends only on the gluino mass, the quark–antiquark initiated matrix element in (11) involves also quarks and squarks and thus depends also on the masses of these (s)particles. Since we are working in the collinear limit at high center-of-mass energies, we neglect the masses of the five light initial quark and antiquark flavors and take their momentum distributions inside the photon, $f_{i/\gamma}(x, M^2)$, from a leading-order, five-flavor fit to the photon structure function [35]. For center-of-mass energies $\sqrt{s}_{\gamma\gamma} > 2(m_t + m_{\tilde{g}}) > 748.6\,\mathrm{GeV}$ (relevant for $m_{\tilde{g}} > 200\,\mathrm{GeV}$), top quarks can contribute through the process $\gamma\gamma \to t\bar{t}\tilde{g}\tilde{g}$ at $\mathcal{O}(\alpha^2\alpha_s^2)$. While this process is of the same order as the direct contributions considered in the previous section, it is phase-space suppressed by the larger mass of the final state and will therefore be neglected.

In Fig. 9, the direct contribution (dashed curve) falls steeply with the squark mass parameter $m_{\rm SUSY}$, while the small resolved gluon–gluon initiated channel (dot-dashed curve) is, of course, independent of the squark mass. Interestingly, the resolved quark–antiquark initiated contribution, which coincides with the total resolved cross section

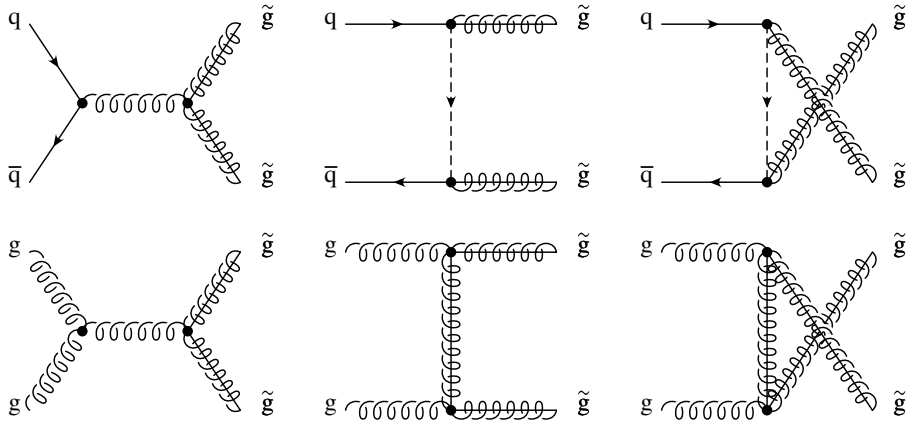

Fig. 7. Feynman diagrams for gluino pair production in quark–antiquark collisions

Fig. 8. Feynman diagrams for gluino pair production in gluon–gluon collisions

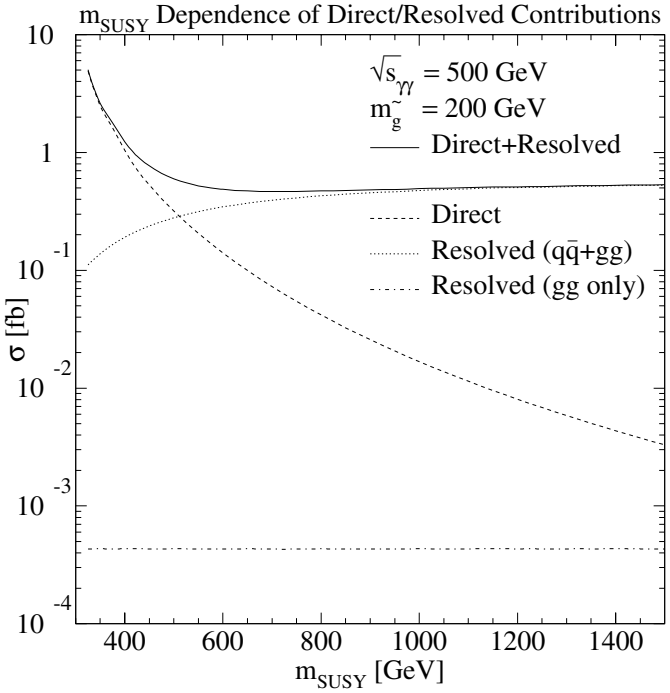

Fig. 9. Dependence of the direct, resolved, and gg initial state contributions to the gluino pair production cross section in unpolarized photon–photon collisions on the squark mass parameter $m_{\rm SUSY}$

(dotted curve), increases with $m_{\rm SUSY}$. The reason is that the s- and t-channel diagrams in Fig. 7 interfere destructively, and the interference contributions to (11) decrease in magnitude as $m_{\rm SUSY}$ increases. As a consequence, the total gluino pair production cross section (full curve) remains large even for large squark masses and becomes independent of $m_{\rm SUSY}$ already for moderate squark masses.

Figure 10 shows the threshold behavior of the direct (dashed curves), quark–antiquark (dotted curves), and gluon–gluon initiated cross sections (dot-dashed curves) for small (top) and large (bottom) values of $m_{\rm SUSY}$. In the first scenario, the direct channel dominates at threshold as expected, while in the second case it is completely negligible in the entire center-of-mass energy range. Instead, the threshold behavior of the total cross section is dominated by the quark–antiquark channel, and the gluon–gluon process contributes significantly at larger values of $\sqrt{s}_{\gamma\gamma}$.

Resolved contributions are therefore only important (1) if $\sqrt{s}_{\gamma\gamma} \gg 2m_{\tilde{g}}$, i.e. far above the gluino pair production threshold, or (2) if $m_{\tilde{q}} \gg m_{\tilde{g}}$. The first case is of little practical importance. For $m_{\tilde{q}} \leq m_{\tilde{g}}$, it would in fact be desirable to suppress the resolved contributions so that the photon–photon center-of-mass energy is fully available in threshold scans. This should be feasible by reconstructing the observed momentum fractions of the partons in the photon from the gluino pair and requiring them to be large. The second case is more interesting and may allow for a gluino mass determination in scenarios that would be unobservable in e^+e^- or direct $\gamma\gamma$ collisions.

4 Polarized electron–electron scattering

In practice, high-energy photon collisions will become feasible through the backscattering of laser photons from electron beams at future linear colliders. The unpolarized and polarized laser backscattering spectra are [21]

$$f_{\gamma/e}(x) = \frac{1}{N_c + 2\lambda_e P_c N_c'} \times \left\{1 - x + \frac{1}{1-x} - \frac{4x}{X(1-x)} + \frac{4x^2}{X^2(1-x)^2} - 2\lambda_e P_c \frac{x(2-x)[x(X+2)-X]}{X(1-x)^2}\right\} \quad (14)$$

and

$$\Delta f_{\gamma/e}(x) = \frac{1}{N_c + 2\lambda_e P_c N_c'} \times \left\{2\lambda_e \frac{x}{1-x}\left[1 + (1-x)\left(1 - \frac{2x}{(1-x)X}\right)^2\right] + P_c\left(1 - \frac{2x}{(1-x)X}\right)\left(1 - x + \frac{1}{1-x}\right)\right\}, \quad (15)$$

where

$$N_c = \left[1 - \frac{4}{X} - \frac{8}{X^2}\right]\ln(1+X) + \frac{1}{2} + \frac{8}{X} - \frac{1}{2(1+X)^2} \quad (16)$$

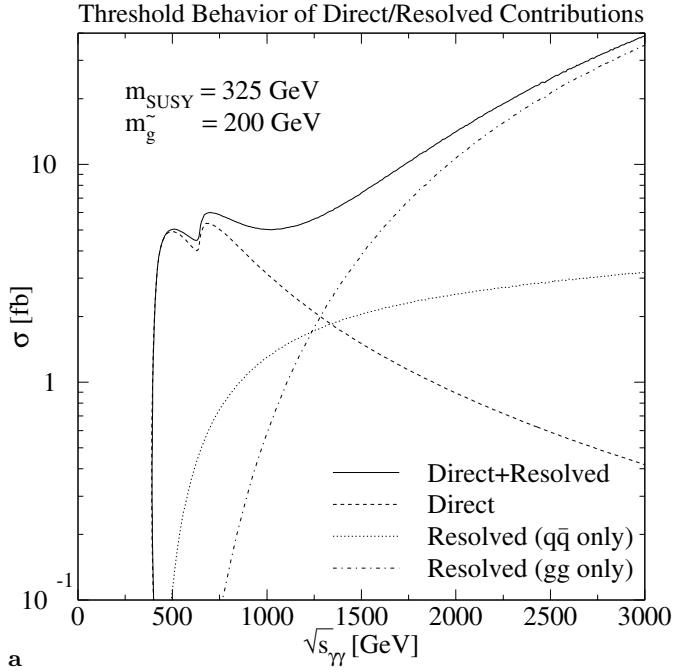

Fig. 10. Threshold behavior of the direct, $q\bar{q}$, and gg initial state contributions to the gluino pair production cross section in unpolarized photon–photon collisions for a small (upper plot) and large (lower plot) squark mass parameter $m_{\rm SUSY}$

and

$$N_c' = \left[\left(1+\frac{2}{X}\right)\ln(1+X) - \frac{5}{2} + \frac{1}{1+X} - \frac{1}{2(1+X)^2}\right] \quad (17)$$

are related to the total Compton cross section and $\xi_i = \Delta f_{\gamma/e}(x_i)/f_{\gamma/e}(x_i)$ is the mean helicity of the backscattered photon i.

The photon spectra depend on the center-of-mass energy of the electron-laser photon collision $s_{e\gamma}$ through the parameter $X = s_{e\gamma}/m_e^2 - 1$, whose optimal value is determined by the threshold for e^+e^- pair production. In the strong fields of the laser waves, the electrons (or high-energy photons) can interact simultaneously with several laser photons, so that the optimal value of X increases from $(2+\sqrt{8})$ to $(2+\sqrt{8})(1+\xi^2) \simeq 6.5$ [36]. If the parameter X is kept fixed, the laser backscattering spectra become independent of the electron beam energy. A large fraction of the photons is then produced close to the kinematic limit $x < x_{\rm max} = X/(X+1) = 0.8\bar{6}$. The monochromaticity of the produced photons can be improved further by choosing the helicity of the 100% polarized laser photons opposite to that of the 80% polarized electrons.

Since the low-energy tail of the photon spectrum is neither useful nor well understood, we use only the high-energy peak with $x > 0.8\,x_{\rm max} = 0.69\bar{3}$, where $x = \sqrt{s_{\gamma\gamma}/s_{ee}}$, and normalize our cross sections by the corresponding fraction of the partonic photon–photon luminosity (29.1%), so that the expected number of events can be obtained through simple multiplication with the envisaged photon–photon luminosity of 100–200 fb^{-1}/year. This requires reconstruction of the total final-state energy, which may be difficult due to the missing energy carried away by the (typically two) escaping lightest SUSY particles (LSPs). However, high-energy photon collisions allow for cuts on the relative longitudinal energy in addition to the missing-E_T plus multi-jet, top or bottom quark, and/or like-sign lepton analyses performed at hadron colliders, and sufficiently long-lived gluinos can be identified by their typical R-hadron signatures.

The total cross section for gluino pair production in polarized electron–electron collisions is given by

$$\begin{aligned}\sigma_{ee} = \int {\rm d}x_1 f_{\gamma/e}(x_1){\rm d}x_2 f_{\gamma/e}(x_2){\rm d}t_{\tilde{g}} \\ \times \left[\frac{1}{2}(1+\xi_1)(1+\xi_2)\frac{{\rm d}\sigma_{\rm dir}^{++}}{{\rm d}t_{\tilde{g}}}\right. \\ + \frac{1}{2}(1+\xi_1)(1-\xi_2)\frac{{\rm d}\sigma_{\rm dir}^{+-}}{{\rm d}t_{\tilde{g}}} \\ + \frac{1}{2}(1-\xi_1)(1+\xi_2)\frac{{\rm d}\sigma_{\rm dir}^{-+}}{{\rm d}t_{\tilde{g}}} \\ \left. + \frac{1}{2}(1-\xi_1)(1-\xi_2)\frac{{\rm d}\sigma_{\rm dir}^{--}}{{\rm d}t_{\tilde{g}}}\right], \end{aligned} \quad (18)$$

where parity conservation in (SUSY-)QCD guarantees that $\sigma_{\rm dir}^{++} = \sigma_{\rm dir}^{--}$ and $\sigma_{\rm dir}^{+-} = \sigma_{\rm dir}^{-+}$. For resolved processes, the photon densities are replaced by parton densities in the electron,

$$f_{a/e}(x,M^2) = \int_x^1 \frac{{\rm d}y}{y} \quad f_{\gamma/e}\left(\frac{x}{y}\right) \quad f_{a/\gamma}(y,M^2) \quad (19)$$

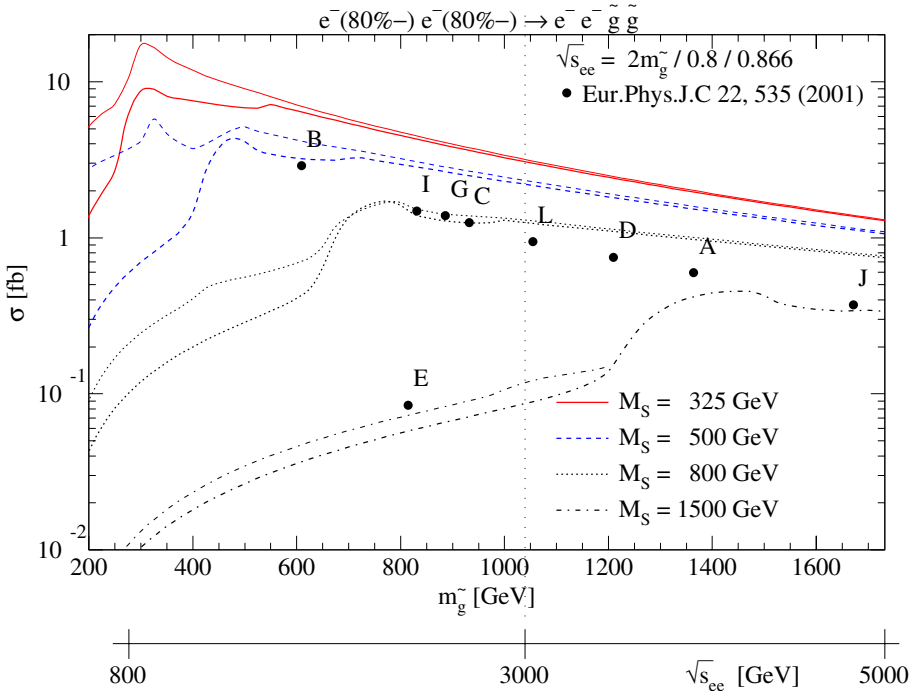

Fig. 11. Dependence of the gluino pair production cross section in $\gamma\gamma$ collisions on the universal squark mass $m_{\rm SUSY}$ for no squark mixing (thick curves) and maximal top-squark mixing (thin curves). The e^-e^- center-of-mass energy is chosen close to the threshold for gluino pair production and is varied simultaneously with $m_{\tilde{g}}$. Also shown are the cross sections expected for the post-LEP SUSY benchmark points in [37] (full points)

and

$$\Delta f_{a/e}(x, M^2) = \int_x^1 \frac{\mathrm{d}y}{y} \Delta f_{\gamma/e}\left(\frac{x}{y}\right) \Delta f_{a/\gamma}(y, M^2). \quad (20)$$

In Fig. 11 we show that gluino pair production in direct $\gamma\gamma$ collisions decreases with the universal squark mass $m_{\rm SUSY}$, but depends only weakly on the top-squark mixing. This is in sharp contrast to the results obtained in e^+e^- annihilation [11,12]. In this plot, the e^-e^- center-of-mass energy is chosen close to the threshold for gluino pair production ($\sqrt{s} = 2m_{\tilde{g}}/0.8/0.8\bar{6}$) and is varied simultaneously with $m_{\tilde{g}}$. Also shown in Fig. 11 are several post-LEP SUSY benchmark points, which have recently been proposed within the framework of the constrained MSSM [37]. Studies similar to those performed in Fig. 13 show that with the exception of point E, where only about ten events per year are to be expected, the gluino mass can be determined with a precision of ±20 GeV (point J) or better.

For gluino masses between 200 and 500 GeV, the total cross section for gluino pair production in polarized electron–electron collisions with laser backscattered photons is shown in Fig. 12 as a function of the electron–electron center-of-mass energy $\sqrt{s}_{ee}$. The corresponding e^+e^- annihilation cross section stays below 0.1 fb and falls steeply with $m_{\tilde{g}}$, so that gluino pair production will be unobservable for $m_{\tilde{g}} > 500$ GeV irrespective of the collider energy [11,12]. In contrast, the $\gamma\gamma$ cross section reaches several fb for a wide range of $m_{\tilde{g}}$. In e^+e^- annihilation the gluinos are produced as a P-wave and the cross section rises rather slowly, whereas in $\gamma\gamma$ collisions they can be produced as an S-wave and the cross section rises much faster. This is particularly true for identical helicities of the initial photons (see Fig. 4).

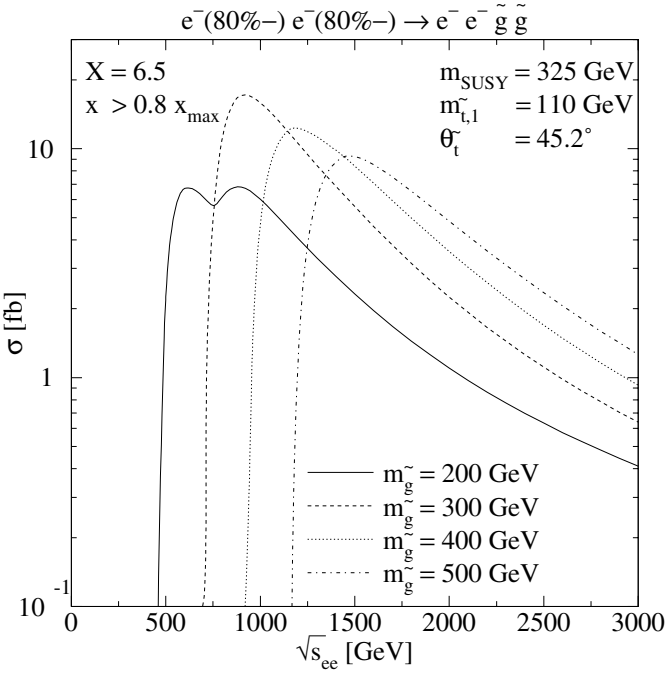

Fig. 12. The gluino pair production cross section in polarized direct photon collisions as a function of the e^-e^- center-of-mass energy for various gluino masses. The partonic photon–photon luminosity has been normalized to unity in the high-energy peak

The steep threshold behavior can be observed even more clearly in Fig. 13, where the sensitivity of a photon collider to the gluino mass is investigated. For the CERN LHC experiments, a precision of ±30 ... 60 (12 ... 25) GeV is expected for gluino masses of 540 (1004) GeV [8,9]. If

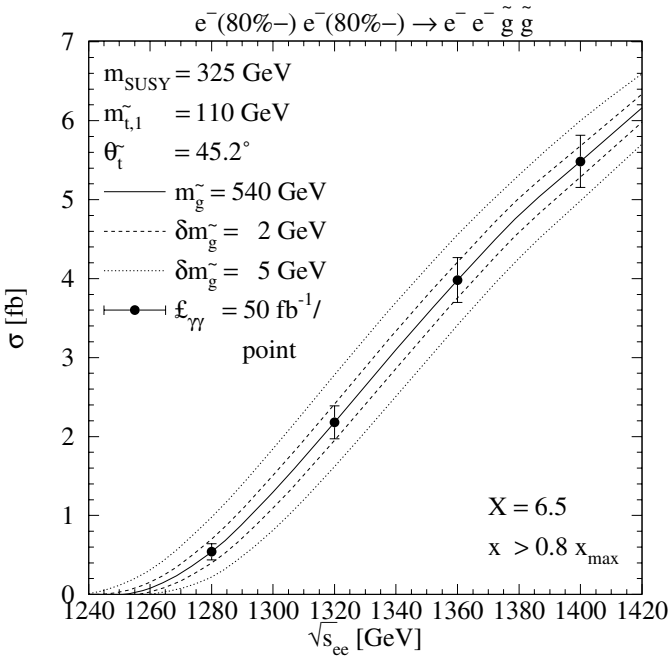

Fig. 13. Sensitivity of the gluino pair production cross section in polarized direct photon collisions to the mass of the pair-produced gluino. The partonic photon–photon luminosity has been normalized to unity in the high-energy peak

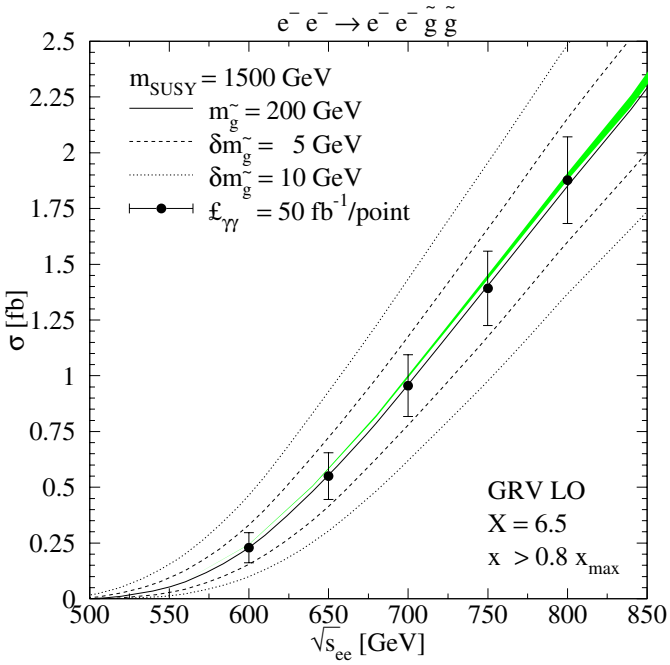

Fig. 14. Sensitivity of the gluino pair production cross section in unpolarized resolved photon collisions to the mass of the pair-produced gluino. The unpolarized partonic photon–photon luminosity has been normalized to unity in the high-energy peak, which corresponds to 18.9% of the total

the masses and mixing angle(s) of the top (and bottom) squarks are known, a statistical precision of $\pm 5 \ldots 10\,\mathrm{GeV}$ can be achieved in e^+e^- annihilation for $m_{\tilde{g}} = 200\,\mathrm{GeV}$ for an integrated luminosity of $100\,\mathrm{fb}^{-1}$ per center-of-mass energy point [11,12]. A precision of $\pm 2 \ldots 5\,\mathrm{GeV}$ may be obtained at a TeV-scale photon collider for $m_{\tilde{g}} = 540\,\mathrm{GeV}$ and an integrated photon–photon luminosity of $50\,\mathrm{fb}^{-1}$ per point, provided that the total final-state energy can be sufficiently well reconstructed. Of course, uncertainties from a realistic photon spectrum and the detector simulation add to the statistical error.

In Fig. 14 we demonstrate that even in scenarios with a very large squark mass parameter $m_{\mathrm{SUSY}} = 1500\,\mathrm{GeV}$ and no squark mixing a gluino mass of $m_{\tilde{g}} = 200\,\mathrm{GeV}$ could be determined with a precision of $\pm 5 \ldots 10\,\mathrm{GeV}$. The cross section is then dominated by the quark initiated resolved contributions (see the lower plot in Fig. 10). The shaded band indicates the uncertainty from a variation of parton densities in the photon from GRV LO [35] to SaS 1D and 1M [38]. It turns out to be fairly small, since the quark densities at large x are well constrained from photon structure function data [39].

5 Conclusions

In conclusion, the reconstruction of the SUSY Lagrangian and the precise determination of its free parameters are among the paramount objectives of any future linear e^+e^- collider. Determination of the gluino mass and coupling will, however, be difficult, since the gluino couples only strongly and its pair production cross section in e^+e^- annihilation suffers from large cancellations in the triangular quark/squark loop diagrams. A photon collider may therefore be the only way to obtain precise gluino mass determinations and visible gluino pair production cross sections for general squark masses and would thus strongly complement the physics program feasible in e^+e^- annihilation. For recently proposed typical post-LEP SUSY benchmark points, gluino pairs can be produced from laser backscattered photons with cross sections between 0.1 fb and 4 fb, so that a gluino mass of 540 (1670) GeV may be determined with a precision of $\pm 2 \ldots 5$ (± 20) GeV or better.

Acknowledgements. We thank A. de Roeck for bringing [37] to our attention and B.A. Kniehl and G. Kramer for a careful reading of the manuscript. This work has been supported by Deutsche Forschungsgemeinschaft through Grant No. KL 1266/1-3 and through Graduiertenkolleg Zukünftige Entwicklungen in der Teilchenphysik.

References

1. H.P. Nilles, Phys. Rept. **110**, 1 (1984)
2. H.E. Haber, G.L. Kane, Phys. Rept. **117**, 75 (1985)
3. M. Carena et al. [Higgs Working Group Collaboration], hep-ph/0010338
4. S. Abel et al. [SUGRA Working Group Collaboration], hep-ph/0003154
5. R. Culbertson et al. [Gauge Mediation Working Group Collaboration], hep-ph/0008070
6. S. Ambrosanio et al. [BMSSM Working Group Collaboration], hep-ph/0006162

7. B. Allanach et al. [RPV Working Group Collaboration], hep-ph/9906224
8. A. Airapetian et al. [ATLAS Collaboration], CERN-LHCC-99-15
9. S. Abdullin et al. [CMS Collaboration], J. Phys. G **28**, 469 (2002)
10. J.A. Aguilar-Saavedra et al. [ECFA/DESY LC Physics Working Group Collaboration], hep-ph/0106315
11. S. Berge, M. Klasen, Phys. Rev. D **66**, 115014 (2002)
12. S. Berge, M. Klasen, contribution to SUSY 02, hep-ph/0210420
13. G. Jikia, S. Söldner-Rembold, Nucl. Phys. Proc. Suppl. **82**, 373 (2000)
14. M. Melles, W.J. Stirling, V.A. Khoze, Phys. Rev. D **61**, 054015 (2000)
15. P. Niezurawski, A.F. Zarnecki, M. Krawczyk, Acta Phys. Polon. B **34**, 177 (2003)
16. M.M. Mühlleitner, M. Krämer, M. Spira, P.M. Zerwas, Phys. Lett. B **508**, 311 (2001)
17. S. Chakrabarti, D. Choudhury, R.M. Godbole, B. Mukhopadhyaya, Phys. Lett. B **434**, 347 (1998)
18. S. Berge, M. Klasen, Y. Umeda, Phys. Rev. D **63**, 035003 (2001)
19. M. Klasen, Nucl. Instrum. Meth. A **472**, 160 (2001)
20. B. Badelek et al. [ECFA/DESY Photon Collider Working Group Collaboration], hep-ex/0108012
21. I.F. Ginzburg, G.L. Kotkin, S.L. Panfil, V.G. Serbo, V.I. Telnov, Nucl. Instrum. Meth. A **219**, 5 (1984)
22. K. Hagiwara et al. [Particle Data Group Collaboration], Phys. Rev. D **66**, 010001 (2002)
23. T. Affolder et al. [CDF Collaboration], Phys. Rev. Lett. **88**, 041801 (2002)
24. S. Abachi et al. [D0 Collaboration], Phys. Rev. Lett. **75**, 618 (1995)
25. M. Felcini, C. Tully et al. [LEP Higgs Working Group Collaboration], Note 2001-04, hep-ex/0107030
26. T. Hahn, C. Schappacher, Comput. Phys. Commun. **143**, 54 (2002)
27. J. Abdallah et al. [LEP SUSY Working Group Collaboration], http://lepsusy.web.cern.ch/lepsusy
28. J. Küblbeck, M. Böhm, A. Denner, Comput. Phys. Commun. **60**, 165 (1990)
29. T. Hahn, Comput. Phys. Commun. **140**, 418 (2001)
30. G.J. van Oldenborgh, J.A. Vermaseren, Z. Phys. C **46**, 425 (1990)
31. G.J. van Oldenborgh, Comput. Phys. Commun. **66**, 1 (1991)
32. T. Hahn, M. Perez-Victoria, Comput. Phys. Commun. **118**, 153 (1999)
33. S.P. Li, H.C. Liu, D. Silverman, Phys. Rev. D **31**, 1736 (1985)
34. S. Dawson, E. Eichten, C. Quigg, Phys. Rev. D **31**, 1581 (1985)
35. M. Glück, E. Reya, A. Vogt, Phys. Rev. D **46**, 1973 (1992)
36. H. Burkhardt, V. Telnov, CERN-SL-2002-013-AP
37. M. Battaglia et al., Eur. Phys. J. C **22**, 535 (2001)
38. G.A. Schuler, T. Sjostrand, Z. Phys. C **68**, 607 (1995)
39. M. Klasen, Rev. Mod. Phys. **74**, 1221 (2002)